

# Self-Assembly of Biofunctional Polymer on Graphene Nanoribbons

Darkeyah G. Reuven, Kelvin Suggs, Michael D. Williams, and Xiao-Qian Wang\*

Department of Physics and Center for Functional Nanoscale Materials, Clark Atlanta University, Atlanta, Georgia 30314, United States

The planar structure of graphene has potential applications in electronics, sensor devices, spintronics, nanoelectronics, and biodiagnostics.<sup>1–5</sup> Laterally constraining the carriers in a quasi-one-dimensional system, graphene nanoribbons (GNRs) can be fabricated using lithographic methods<sup>6–8</sup> and by metal particle-assisted<sup>9–11</sup> or oxidative<sup>12,13</sup> longitudinal unzipping of multiwalled carbon nanotubes (MWCNTs). Oxidative chemistry-produced GNRs can be processed for specific applications by modification of the basal plane and edge functional groups composed of carboxylic acid, hydroxyl, epoxide, and carbonyl. Hydrazine significantly reduces the amount of oxygen functional groups on GNRs, resulting in improved conductivity.<sup>12,13</sup>

Recently, significant efforts have been devised to create self-assembled hierarchical graphene-based materials.<sup>14–16</sup> Examples include the co-assembly of graphene and organic monolayer,<sup>17,18</sup> titania nanosheets,<sup>13</sup> and proteins.<sup>16</sup> These ordered structures are assembled by intermolecular forces arising from electrostatic,  $\pi-\pi$  stacking, dipolar, van der Waals, hydrogen bonding, or metal–ligand interactions. Various types of polymers have been shown to interact with graphene<sup>19</sup> or graphene oxide, forming stable hybrids.<sup>15,17</sup> For instance, modified poly(phenylene vinylene) conductive polymer can specifically attach to GNRs and tune the corresponding electronic properties.<sup>20</sup> In view of the rapid progress made in preparing controlled polymer self-assembly, a better understanding of the interfacial interactions between the helical polymer and GNRs is clearly desirable.

## RESULTS AND DISCUSSION

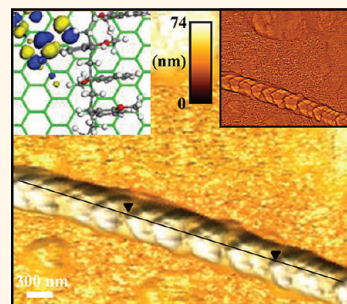
We have investigated the self-assembly of biocompatible polymer,  $\alpha,\omega$ -bi[2,4-dinitrophenyl caproic] [poly(ethylene oxide)-*b*-poly(2-methoxystyrene)-*b*-poly(ethylene oxide)] (DNP-PEO-P2MS-PEO-DNP, hereafter referred to as *m*-P2MS), onto chemically prepared

**ABSTRACT** Graphene's adhesive properties owing to inherent van der Waals interactions become increasingly relevant in the nanoscale regime. Polymer self-assembly *via* graphene-mediated noncovalent interactions offers a powerful tool for the creation of anisotropic nanopatterned systems. Here, we report the supramolecular self-assembly of biofunctional-modified poly(2-methoxystyrene)

on graphene nanoribbons prepared by unzipping multiwalled carbon nanotubes. This approach promotes the glycol-modified polymer to self-assemble into structured nanopatterns with preserved bioactivity. The self-assembly is attributed to enhanced van der Waals interactions and the associated charge transfer from polymer to graphene. These findings demonstrate that the assembly yields a prospective route to novel nanomaterial systems.

**KEYWORDS:** graphene nanoribbons · self-assembly · nanomaterials · polymer · biofunctional

GNRs. P2MS polymer with more than 20 2-methoxystyrene monomers forms a helix rod structure.<sup>21</sup> *m*-P2MS assembles into secondary structures in solution, resulting in associated optical activity.<sup>22</sup> Furthermore, the chiral initiated polymer surfaces are better supports for HeLa, mouse osteoblast, and human osteoblast cell as compared to nonchiral initiated counterparts, owing to the moderately periodic topography.<sup>23</sup> Dinitrophenol groups attached at the ends of *m*-P2MS are suitable for biosensing applications due to their high affinity to anti-DNP IgE protein in solution and IgE on the surface of mast cells.<sup>24</sup> The dangling glycol end-segment is hydrophilic, aiding in the extension of the DNP groups away from the P2MS backbone in aqueous environments, thereby assisting DNP's availability for protein interaction. However, *m*-P2MS typically forms nonuniform surfaces upon deposition on substrates. The lack of control in the formation of uniform surfaces hinders the application of this type of versatile polymer. In this regard, the hierarchal self-assembly of *m*-P2MS into anisotropic ordered patterns



\* Address correspondence to xwang@cau.edu.

Received for review December 9, 2011 and accepted January 11, 2012.

Published online January 11, 2012  
10.1021/nn204825b

© 2012 American Chemical Society

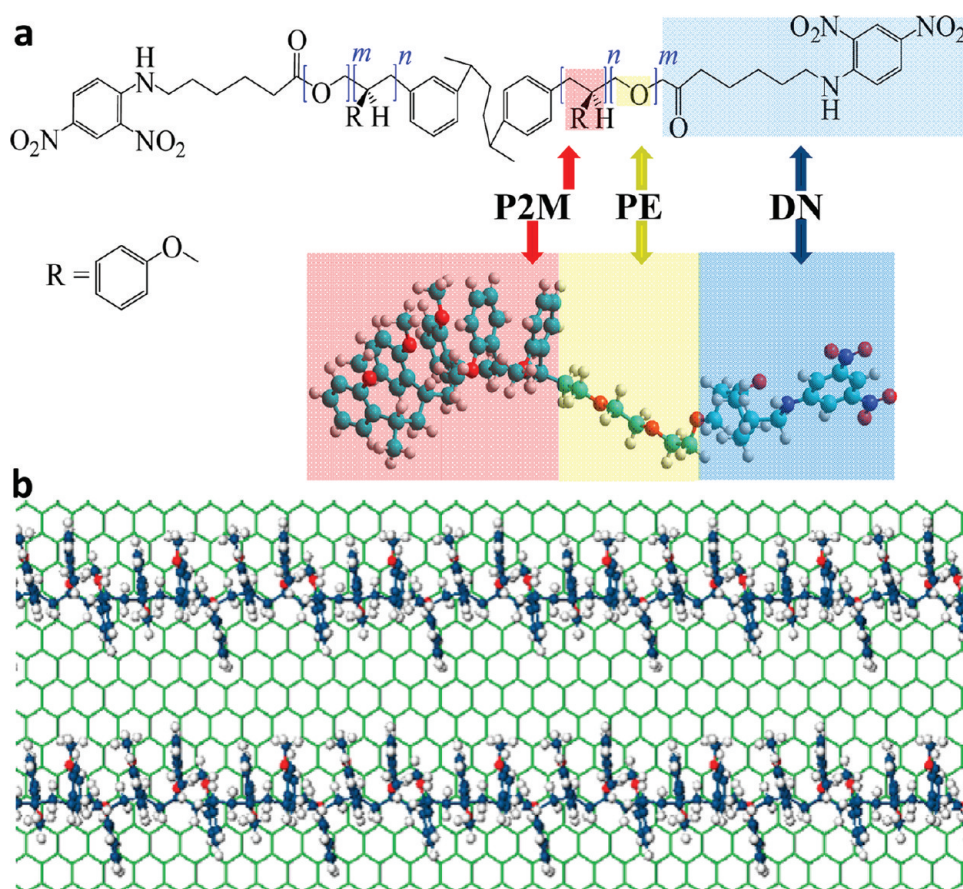


**Figure 1.** *m*-P2MS chemical scheme and optimized geometry. (a) Schematic representation of  $\alpha,\omega$ -bi[2,4-dinitrophenyl caproic] [poly(ethylene oxide)-*b*-poly(2-methoxystyrene)-*b*-poly(ethylene oxide)] (*m*-P2MS), and side views of optimized helical *m*-P2MS section. Helical poly(2-methoxystyrene), glycol segment, and pendant 2,4-dinitrophenyl are highlighted in red, yellow, and blue, respectively. (b) Top view of the optimized structure of attached helically P2MS on graphene (green color).

on chemically prepared GNRs is timely and of considerable interest. This is particularly the case because surface-adsorbed *m*-P2MS–GNR specifically binds with anti-DNP IgE protein.

Illustrated in Figure 1 is chemical scheme of *m*-P2MS, along with optimized geometries of *m*-P2MS and parallel aligned P2MS chains on graphene (Supporting Information, Figures S3, S4, and S5). While the electronic structure for graphene and GNRs is distinctive from each other, the ensuing changes arising from the GNR edges become dormant for ribbons with a width larger than 100 nm. Monomers of 2-methoxystyrene in Figure 1a were optimized using dispersion-corrected density functional theory (DFT) method (Supporting Information). First-principles calculation results show that helical P2MS aligns parallel on graphene owing to van der Waals interactions (Figure 1b and Supporting Information). The calculated electronic band structure of *m*-P2MS-functionalized graphene shows substantial molecular orbital hybridization, which indicates component charge transfers (Supporting Information, Figure S3). Specifically, 2-methoxystyrene monomers in the polymer backbone serve as charge donors to graphene. Consequently, the helical *m*-P2MS chains

and graphene form donor–acceptor complex with enhanced van der Waals interactions. The diameter of *m*-P2MS backbone is about 5 nm. As a result, GNRs generated from unzipping MWCNTs, with typical width of 300–500 nm and length of a few micrometers, provide desired planar “flatbed” for *m*-P2MS self-assembly. Furthermore, the oxygen groups at the GNR edge and the basal plane contribute to *m*-P2MS self-assembly onto GNRs *via* hydrogen bonding.

*m*-P2MS of 10–15K molecular weight (74–112 repeat units) forms aggregates of  $265 \pm 35$  nm diameters in tetrahydrofuran (THF) solvent, which was confirmed by dynamic light scattering (DLS) (Supporting Information, Figure S6). The strong van der Waals interactions between the *m*-P2MS helical rigid rods lead to the formation of polymer-specific sized aggregates in solution. The optical rotation of polarized light by the *m*-P2MS secondary polymer structures in solution, yet the formation of nonuniform films on silicon or silicon oxide surfaces, indicates that aggregates form weakly associated superstructures in solution. As such, GNR's adhesive properties, due to its inherent van der Waals forces,<sup>25</sup> make it suitable for the controlled attachment of *m*-P2MS secondary polymer structures, which is of

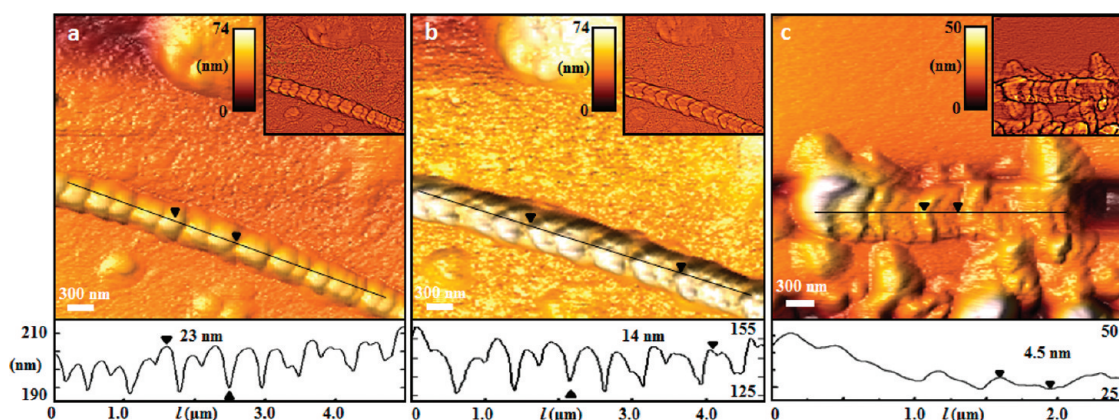


**Figure 2.** Supramolecular organization of polymer features on GNR. Three-dimensional rendering of AFM topography data, along with the contrast enhanced image by multiscale gradient transformation of P2MS–GNR hybrid at various stages of processing. (a) Lamella ordered *m*-P2MS polymer drop-cast on the GNR. The gradient transformed image of partially overlapping polymer lamella in scale like fashion. Bottom insets: structured polymer periodicity of  $\sim 200$  nm and height of  $\sim 75$  nm along the *m*-P2MS–GNR hybrid, before and after solvent treatment. (b) Aligned herringbone-shaped lamella polymer features after 24 h exposure to solvent-rich environment. Inset: gradient transformed image with the herringbone shapes. Bottom insets: structured polymer periodicity of  $\sim 195$  nm and height of  $\sim 75$  nm along the *m*-P2MS–GNR hybrid. (c) Aligned herringbone-shaped polymer features in polymer deposited on chemically reduced GNR (*r*-GNR). Bottom insets: structured polymer periodicity of  $\sim 150$  nm with heights of 4.5–20 nm extracted from the height profile along the *m*-P2MS–*r*-GNR hybrid.

interest from the perspective of better understanding graphene/polymer nanoscale film topography.

To this effect, we have prepared GNRs with a typical height of approximately 0.50–0.75 nm using oxidative chemistry technique developed by Tour and co-workers (Supporting Information, Figures S1 and S2).<sup>12,13</sup> We show in Figure 2 typical atomic force microscopy (AFM) images of *m*-P2MS spin-cast onto single-layer GNR adsorbed on a SiO<sub>2</sub> surface. The *m*-P2MS polymer spontaneously self-assembles along the entire ribbon in a platelet pattern (Figure 2a). The platelet nanopattern has a periodicity of  $200 \pm 20$  nm and an overall height of 59–74 nm. The mean corrugation height along the cross section of the hybrid ribbon is  $23 \pm 5$  nm (Figure 2a). The gradient processed image (inset of Figure 2a) displays partially overlapping polymer lamella in “scale like” fashion along the GNR. The size of apparent platelet pattern is consistent with DLS data that reveal similarly sized *m*-P2MS aggregates in THF solvent. This demonstrates that the  $\sim 265$  nm *m*-P2MS secondary polymer structures attach to the graphene surface *via* electrostatic and van der Waals interactions, forming supramolecular layers and presumably further mediated by the graphene edges. In contrast, there are no distinguishable ordered *m*-P2MS polymer structures on the amorphous SiO<sub>2</sub> surface (Figure 2a).

The nanocomposites were processed to form complex networks upon further exposure to a solvent vapor-rich atmosphere for a 12 h period (Figure 2b). The *m*-P2MS on the GNR spontaneously forms into aligned herringbone features on the GNR. The herringbone pattern has a periodicity of  $200 \pm 20$  nm, along with an overall height and width of 59–74 and 550 nm, respectively. The gradient processed image (inset of Figure 2b) reveals a distinct herringbone pattern on the

ribbon. The average corrugation height along the cross section of the hybrid ribbon is  $14 \pm 5$  nm (inset of Figure 2b), a moderate reduction of film topography after solvent exposure. These herringbone-shaped polymer features are attributed to the incorporation of solvent vapor into the polymer matrix, allowing for increased *m*-P2MS chain mobility. The *m*-P2MS chains are subsequently able to undergo further van der Waals mediated adhesion to the GNR.

The chemical unzipping of MWCNTs invariably leads to the presence of oxygen species on the basal plane and ketone groups along edges of the GNR, which can interact with the ether groups available on the *m*-P2MS aggregate. The combination of the hydrophobic P2MS chain and hydrophilic glycol terminal groups is essential for supramolecular attachment to the GNRs. A circular dichroism spectroscopy study of *m*-P2MS and the hybrid with GNRs reveals that, while the feature of the helical rod of *m*-P2MS is modified slightly with the inclusion of GNRs, the addition of water plays an important role in the enhanced interactions between *m*-P2MS and GNRs (Supporting Information, Figure S10). We demonstrate in Figure 2c the height tuning of the *m*-P2MS polymer nanopattern on chemically reduced GNR (*r*-GNR). A herringbone polymer pattern is clearly evident on *r*-GNR (Figure 2c). The height data (inset of Figure 2c) profile along the P2MS–*r*-GNR hybrid shows the structured polymer periodicity of  $150 \pm 10$  nm and an overall corrugation height ranging from 4.5 to 20 nm. Thus, the reduction in *m*-P2MS surface topology is likely related to the decrease of the oxygen functional groups, while the preservation of the herringbone pattern can be attributed to van der Waals interaction with the GNR. Consequently, *r*-GNR facilitates flexibility in controlling polymer height,

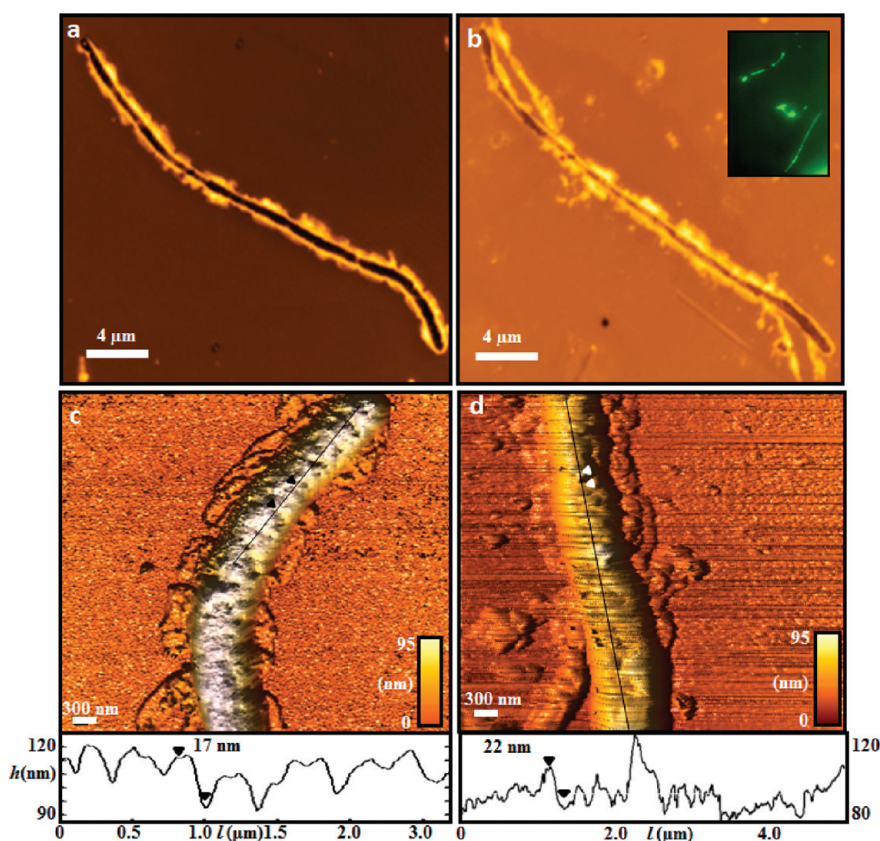


Figure 3. *m*-P2MS polymer ordering on GNR and IgE binding. (a) Laser confocal microscope and 3D rendering of AFM topography image of *m*-P2MS polymer ordering on GNR before (a,c) and after (b,d) IgE exposure, respectively. Inset of b: Fluorescence confocal microscope images.

while retaining the characteristic polymer pattern on the *r*-GNR surface.

The polymer interaction with the GNR nanofiller was investigated using differential scanning calorimetry (DSC) over the temperature range of 40 to 200 °C. The GNR thermogram exhibits an endothermic transition approximately at 130 °C, which is attributed to the release of adsorbed water (Supporting Information, Figure S7a). Upon further heating, the GNRs undergo an exothermic transition at 170 °C that is associated with the thermal decomposition. The DSC thermogram of 1% GNR loaded *m*-P2MS shows a melting temperature at 102 °C, an increase of 7 °C in comparison to *m*-P2MS and *m*-P2MS loaded with 1% *r*-GNR, which have melting temperatures of ~95 °C (Supporting Information, Figure S7b). The addition of low concentrations of *r*-GNRs has little effect on the polymer thermal performance. The prominent endothermic peak of the GNR thermogram is notably absent from the GNR and *r*-GNR polymer composite thermograms. The composite thermograms indicate that the *m*-P2MS polymer hinders the release of water from the GNR surface. The composites undergo exothermic deflagration between 150 and 165 °C. The thermal performance of the composite implies that the incorporation of the chemically prepared GNRs at low concentrations into the *m*-P2MS matrix moderately inhibits the polymer chain

movement, consistent with the effect of other carbon-based fillers on polymer thermal properties.<sup>26–30</sup>

To demonstrate the potential of these polymer nanostructures as a biological interface, we performed protein interaction studies using confocal laser scanning microscopy and AFM. IgE is a well-studied protein known to be involved in the body's immune response. The *m*-P2MS adsorbed on the GNRs retains the bioactivity of the divalent DNP functional groups. Three-dimensional laser scanning microscope and AFM images (Figure 3a,c) show polymer ordering on the basal plane and edges of the GNR. As seen in Figure 3a, the polymeric structures are ordered along the GNR. The darker region along the axis is of higher thickness in comparison to the edges. Discernable polymeric structures yield ovate and overlapping configurations (Figure 3c), forming hierarchical polymer structures at GNR basal and edge interfaces. The ovate polymer structures have an average height, width, and length of 7.8, 336, and 900 nm, respectively. The polymer lamella patterns appear to follow along the smooth edges and basal plane of the macromolecular ribbon. These polymeric structures, attached at the edges, undergo further conformational change into secondary periodic structures on the GNR basal plane.

The bioactivity was investigated by incubating the *m*-P2MS–GNR nanocomposite in phosphate buffer

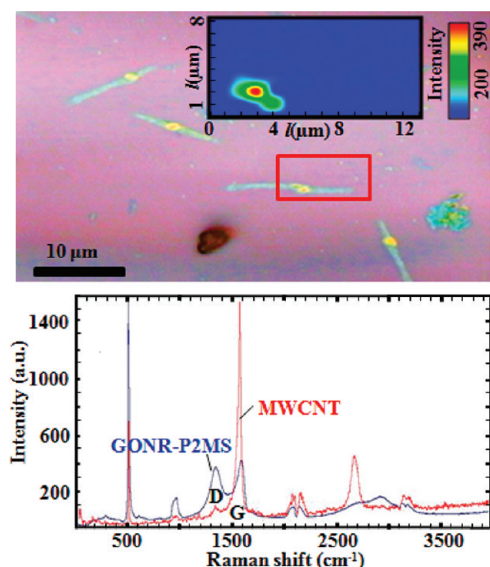


**Figure 4.** Multi-micron polymer ordering on GNR. Long-range polymer ordering of P2MS centered on GNR, propagating on SiO<sub>2</sub>. The composite feature is typically  $\sim 10 \mu\text{m}$  in length and  $\sim 1 \mu\text{m}$  in width. Inset: Micro-Raman map spectroscopy of the peak width of the G ( $1603 \text{ cm}^{-1}$ ) line intensity acquired on a  $12 \times 8 \mu\text{m}^2$  scan window highlighted by the red box.

solution (PBS) containing fluorescently labeled Alexa488-IgE and a blocking protein for 15 min. Fluorescent microscope images (inset of Figure 3b) demonstrate lengthwise fluorescence on the nanocomposite ribbon. Dyes attached to graphene undergo fluorescence resonance energy transfer, which typically results in dye fluorescence quenching.<sup>31,32</sup> By contrast, fluorescence is not quenched in the *m*-P2MS–GNR nanocomposite, as the polymer attached to the GNR surface and edges acts as a spacer that keeps the fluorescently labeled IgE from contacting the GNR surface. AFM topography images in Figure 3d reveal that the IgE protein clusters at the edges of the polymer structures on the GNR. The DNP groups being accessible to anti-DNP IgE in the solid state is relevant for biosensing applications. The features showing IgE protein edge clustering indicate that the DNP groups are spatially confined at the edges of the polymer superstructures and available for protein interactions. It is worth noting that protein fibrils propagate from the edges of the polymer structures. The height profile (inset of Figure 3c) of the P2MS–GNR hybrid shows a periodicity of  $270 \pm 50 \text{ nm}$  and an average corrugation height of  $25 \pm 5 \text{ nm}$ . Subsequent to the IgE exposure, the composite ribbon has a periodicity of  $100 \pm 35 \text{ nm}$  and an average corrugation height of  $15 \pm 5 \text{ nm}$  (inset of Figure 3d). The decrease in surface roughness is attributed to the addition of IgE protein.

A typical Raman spectroscopy (433 nm laser excitation) graph for the GNR polymer hybrid composites a graphene (G) band ( $1603 \text{ cm}^{-1}$ ) and a graphene defect (D) band ( $1354 \text{ cm}^{-1}$ ) of roughly equal

size (Figure 4b). Four bands observed from  $2600$  to  $3200 \text{ cm}^{-1}$  are typical of chemically prepared GNRs.<sup>13</sup> The adsorption of polymer retains the characteristic Raman spectroscopy G band and D band peaks. Shown in Figure 4 is a microscope image of *m*-P2MS/GNR composites, on a silicon oxide substrate, which have been exposed to a solvent atmosphere over a period of a week. Remarkably, the polymer features are spatially confined the approximate width of a GNR (light blue) and anisotropically extend beyond the footprint of the GNRs by several micrometers. Micro-Raman mapping with a spatial resolution of  $1 \mu\text{m}$  was used to investigate the polymer surface features. The Raman mapping of the G line ( $1603 \text{ cm}^{-1}$ ) peak (inset of Figure 4) shows that the center point of the polymer feature (yellow region) is unambiguously assigned to GNRs. These results confirm that the GNRs are capable of controlled propagation of *m*-P2MS over several micrometers on a SiO<sub>2</sub> surface, and the polymer structure retains the approximate width of the nucleating GNR.

Understanding charge transfer at the polymer/graphene interface and the spatial distribution of the resultant charge carriers is important to the development of graphene-based devices. Interestingly, density functional calculations show that charge accumulates at the *m*-P2MS chain ends for the valence band states of the *m*-P2MS–GNR nanocomposite. Graphene preferentially maintains a charge-neutral molecular orbital level.<sup>33–35</sup> Consequently, the energy level alignment relaxation of doped graphene induces optimal charge redistribution from the length of the polymer chain to the *m*-P2MS chain ends, leading to the electrostatic joining of the charged *m*-P2MS chain ends. The induced charge transfer between *m*-P2MS and GNRs promotes long-range attractions, thus allowing the preferred alignment of *m*-P2MS chains. It is worth mentioning that the planar topography and the smooth edges of GNRs play an important role in the self-assembly process. This is in contrast to the deposition of *m*-P2MS on highly ordered pyrolytic graphite (HOPG), in which no regular *m*-P2MS polymer self-assembly pattern is observed (Supporting Information, Figure S9). These observations strongly suggest that GNR facilitates the controlled assembly of *m*-P2MS, owing to enhanced van der Waals interactions and its unique planar conformation with regular edges.

## CONCLUSION

We have described a method for controlled nanopatterning of GNRs by the self-assembly of *m*-P2MS onto the GNR surface. The *m*-P2MS self-assembly on the GNRs is attributed to van der Waals interaction between the GNR basal plane and the *m*-P2MS backbone. The present investigation provides a basis for studying polymer surface topology on GNRs and the associated effect on protein binding.

We remark, before closing, that our approach demonstrates a general strategy for the use of GNRs as a “nano-adhesive tape” for noncovalent fabrication

of functional hybrid nanostructures,<sup>36</sup> which is poised to find use in a variety of practical device applications.

## METHODS

**Nanoribbon Formation.** The MWCNTs were unzipped and reduced using an optimized method developed by Tour and co-workers.<sup>13</sup> A modified GNR purification procedure was utilized, in which the product was isolated by repeated mixing and centrifugation steps, for the separation of exfoliated graphene ribbons from unzipped MWCNTs. The oxidation reaction product was poured into 5 mL of liquid nitrogen cooled 30% hydrogen peroxide, which prevented the precipitation of potassium permanganate. The resultant single and bilayer GNRs were spin-cast from an ethanol/water (50:50) solution onto a silicon wafer with 300 nm SiO<sub>2</sub> wafers. The GNRs were reduced by their adsorption on the SiO<sub>2</sub> surface and subsequent treatment with 1 vol % hydrazine monohydrate and 1 vol % concentrated ammonium hydroxide. The reduced GNRs were washed with deionized water and dried under nitrogen gas flow.

**Protein Binding.** The *m*-P2MS–GNR composites adsorbed on a silicon oxide wafer were sensitized with Alexa488-IgE containing 1 mg/mL of BSA for about 15 min, which were subsequently washed in phosphate buffer solution (PBS) containing BSA.

**Acknowledgment.** The authors are indebted to I. M. Khan, B. Sannigrahi, and B. Baird for providing *m*-P2MS and IgE protein samples. This work was supported by the National Science Foundation (Grants DMR-0934142 and HRD-113757) and Air Force office of Scientific Research (Grant FA9550-10-1-0254). Parts of the analytical studies were performed at Nanotechnology Research Center, Georgia Institute of Technology, a site of the NSF National Nanotechnology Infrastructure Network.

**Supporting Information Available:** Methods, SEM image of unzipped MWCNTs, AFM image of single and bilayer layer GNRs, calculated band structure and extracted charge density distributions of P2MS interacting with graphene, DLS data of *m*-P2MS, DSC thermogram of GNRs and *m*-P2MS–GNR composites, AFM image of *m*-P2MS–GNR–IgE composite, *m*-P2MS deposited on HOPG, and circular dichroism spectroscopy for *m*-P2MS and the *m*-P2MS/GNR composite. This material is available free of charge via the Internet at <http://pubs.acs.org>.

**Conflict of Interest:** The authors declare no competing financial interest.

## REFERENCES AND NOTES

- Chen, Z. H.; Lin, Y. M.; Rooks, M. J.; Avouris, P. Graphene Nano-Ribbon Electronics. *Physica E* **2007**, *40*, 228–232.
- Wang, X.; Ouyang, Y.; Li, X.; Wang, H.; Guo, J.; Dai, H. Room-Temperature All-Semiconducting Sub-10-nm Graphene Nanoribbon Field-Effect Transistors. *Phys. Rev. Lett.* **2008**, *100*, 206803.
- Koenig, S. P.; Boddeti, N. G.; Dunn, M. L.; Bunch, J. S. Ultrastrong Adhesion of Graphene Membranes. *Nat. Nanotechnol.* **2010**, *6*, 543–546.
- Collins, W. R.; Lewandowski, W.; Schmois, E.; Walsh, J.; Swager, T. M. Functionalized Graphenes and Thermoplastic Nanocomposites Based upon Expanded Graphite Oxide. *Angew. Chem., Int. Ed.* **2011**, *50*, 8848–8852.
- Sprinkle, M.; Ruan, M.; Hu, Y.; Hankinson, J.; Rubio-Roy, M.; Zhang, B.; Wu, X.; Berger, C.; de Heer, W. A. Scalable Templated Growth of Graphene Nanoribbons on SiC. *Nat. Nanotechnol.* **2010**, *5*, 727–731.
- Wang, X.; Dai, H. Etching and Narrowing of Graphene from the Edges. *Nat. Chem.* **2010**, *2*, 661–665.
- Han, M. Y.; Ozyilmaz, B.; Zhang, Y. B.; Kim, P. Energy Band-Gap Engineering of Graphene Nanoribbons. *Phys. Rev. Lett.* **2007**, *98*, 206805.
- Tapaszto, L.; Dobrik, G.; Lambin, P.; Biro, L. P. Tailoring the Atomic Structure of Graphene Nanoribbons by Scanning Tunneling Microscope Lithography. *Nat. Nanotechnol.* **2008**, *3*, 397–401.
- Datta, S. S.; Strachan, D. R.; Khamis, S. M.; Johnson, A. T. C. Crystallographic Etching of Few-Layer Graphene. *Nano Lett.* **2008**, *8*, 1912–1915.
- Kim, K.; Sussman, A.; Zettl, A. Graphene Nanoribbons Obtained by Electrically Unwrapping Carbon Nanotubes. *ACS Nano* **2010**, *4*, 1362–1366.
- Elias, A. L.; Botello-Mendez, A. R.; Meneses-Rodriguez, D.; Jehova-Gonzalez, V.; Ramirez-Gonzalez, D.; Ci, L.; Munoz-Sandoval, E.; Ajayan, P. M.; Terrones, H.; Terrones, M. Longitudinal Cutting of Pure and Doped Carbon Nanotubes To Form Graphitic Nanoribbons Using Metal Clusters as Nanoscalpels. *Nano Lett.* **2010**, *10*, 366–372.
- Kosynkin, D. V.; Higginbotham, A. L.; Sinitskii, A.; Lomeda, J. R.; Dimiev, A.; Price, B. K.; Tour, J. M. Longitudinal Unzipping of Carbon Nanotubes To Form Graphene Nanoribbons. *Nature* **2009**, *458*, 872–876.
- Higginbotham, A. L.; Kosynkin, D. V.; Sinitskii, A.; Sun, Z.; Tour, J. M. Lower-Defect Graphene Oxide Nanoribbons from Multiwalled Carbon Nanotubes. *ACS Nano* **2010**, *4*, 2059–2069.
- Xu, J.; Wang, K.; Zu, S.-Z.; Han, B.-H.; Wei, Z. Hierarchical Nanocomposites of Polyaniline Nanowire Arrays on Graphene Oxide Sheets with Synergistic Effect for Energy Storage. *ACS Nano* **2010**, *4*, 5019–5026.
- Wang, Q. H.; Hersam, M. C. Room-Temperature Molecular-Resolution Characterization of Self-Assembled Organic Monolayers on Epitaxial Graphene. *Nat. Chem.* **2009**, *1*, 206–211.
- Zeng, Q.; Cheng, J.; Tang, L.; Liu, X.; Liu, Y.; Li, J.; Jiang, J. Self-Assembled Graphene–Enzyme Hierarchical Nanostructures for Electrochemical Biosensing. *Adv. Funct. Mater.* **2010**, *20*, 3366–3372.
- Zhang, T.; Cheng, Z.; Wang, Y.; Li, Z.; Wang, C.; Li, Y.; Fang, Y. Self-Assembled 1-Octadecanethiol Monolayers on Graphene for Mercury Detection. *Nano Lett.* **2010**, *10*, 4738–4741.
- Wang, Q. H.; Hersam, M. C. Characterization and Nanopatterning of Organically Functionalized Graphene with Ultrahigh Vacuum Scanning Tunneling Microscopy. *MRS Bull.* **2011**, *36*, 532–542.
- An, X.; Simmons, T.; Shah, R.; Wolfe, C.; Lewis, K. M.; Washington, M.; Nayak, S. K.; Talapatra, S.; Kar, S. Stable Aqueous Dispersions of Noncovalently Functionalized Graphene from Graphite and Their Multifunctional High-Performance Applications. *Nano Lett.* **2010**, *10*, 4295–4301.
- Nduwimana, A.; Wang, X. Q. Energy Gaps in Supramolecular Functionalized Graphene Nanoribbons. *ACS Nano* **2009**, *3*, 1995–1999.
- Ogunro, O. O.; Karunwi, K.; Khan, I. M.; Wang, X. Q. Chiral Asymmetry of Helical Polymer Nanowires. *J. Phys. Chem. Lett.* **2010**, *1*, 704–707.
- Gordon, K.; Sannigrahi, B.; McGeady, P.; Wang, X. Q.; Mendenhall, J.; Khan, I. M. *J. Biomater. Sci., Polym. Ed.* **2009**, *20*, 2055–2072.
- Sannigrahi, B.; Sil, D.; Baird, B.; Wang, X. Q.; Khan, I. M. Synthesis and Characterization of Bi[2,4-dinitrophenyl (DNP)] Poly(2-methoxystyrene) Functional Polymers. *J. Macromol. Sci. A* **2008**, *45*, 664–671.
- Baird, E. J.; Holowka, D.; Coates, G. W.; Baird, B. *Biochemistry* **2003**, *42*, 12739–12748.
- Koenig, S. P.; Boddeti, N. G.; Dunn, M. L.; Bunch, J. S. *Nat. Nanotechnol.* **2011**, *6*, 543–546.
- Peters, J. E.; Papavassiliou, D. V.; Grady, B. P. Unique Thermal Conductivity Behavior of Single-Walled Carbon

- Nanotube-Polystyrene Composites. *Macromolecules* **2008**, *41*, 7274–7277.
27. Machado, M. A. L.; Valentini, L.; Biagiotti, J.; Kenny, J. M. Thermal and Mechanical Properties of Single-Walled Carbon Nanotubes-Polypropylene Composites Prepared by Melt Processing. *Carbon* **2005**, *43*, 1499–1505.
  28. Fang, M.; Wang, K.; Lu, H.; Yang, Y.; Nutt, S. Single-Layer Graphene Nanosheets with Controlled Grafting of Polymer Chains. *J. Mater. Chem.* **2010**, *20*, 1982–1992.
  29. Fang, M.; Wang, K.; Lu, H.; Yang, Y.; Nutt, S. Covalent Polymer Functionalization of Graphene Nanosheets and Mechanical Properties of Composites. *J. Mater. Chem.* **2009**, *19*, 7098–7105.
  30. Meador, M. A. B.; Capadona, L. A.; McCorkle, L.; Papadopoulos, D. S.; Leventis, N. *Chem. Mater.* **2007**, *19*, 2247–2260.
  31. Kim, J.; Cote, L. J.; Kim, F.; Huang, J. Visualizing Graphene Based Sheets by Fluorescence Quenching Microscopy. *J. Am. Chem. Soc.* **2009**, *132*, 260–267.
  32. Chang, H.; Tang, L.; Wang, Y.; Jiang, J.; Li, J. Graphene Fluorescence Resonance Energy Transfer Aptasensor for the Thrombin Detection. *Anal. Chem.* **2010**, *82*, 2341–2346.
  33. Topsakal, M.; Ciraci, S. Static Charging of Graphene and Graphite Slabs. *Appl. Phys. Lett.* **2011**, *98*, 131908.
  34. Coletti, C.; Riedl, C.; Lee, D. S.; Krauss, B.; Patthey, L.; von Klitzing, K.; Smet, J. H.; Starke, U. Charge Neutrality and Band-Gap Tuning of Epitaxial Graphene on SiC by Molecular Doping. *Phys. Rev. B* **2010**, *81*, 235401.
  35. Bostwick, A.; Speck, F.; Seyller, T.; Horn, K.; Polini, M.; Asgari, R.; MacDonald, A. H.; Rotenberg, E. Observation of Plasmarons in Quasi-Freestanding Doped Graphene. *Science* **2010**, *328*, 999–1002.
  36. Koenig, S. P.; Boddeti, N. G.; Dunn, M. L.; Bunch, J. S. Ultrastrong Adhesion of Graphene Membranes. *Nat. Nanotechnol* **2011**, *6*, 543–546.